Available online at www.sciencedirect.com
ScienceDirect
Journal of Sound and Vibration 305 (2007) 194–210
JOURNAL OF SOUND AND VIBRATION
www.elsevier.com/locate/jsvi

The strain-based beam finite elements in multibody dynamics

M. Gams, I. Planinc, M. Saje*

Faculty of Civil and Geodetic Engineering, University of Ljubljana, Jamova 2, SI-1115 Ljubljana, Slovenia

Received 24 March 2006; received in revised form 15 March 2007; accepted 28 March 2007
Available online 25 May 2007

Abstract

We present a strain-based finite-element formulation for the dynamic analysis of flexible elastic planar multibody systems, composed of planar beams. We consider finite displacements, rotations and strains. The discrete dynamic equations of motion are obtained by the collocation method. The strains are the basic interpolated variables, which makes the formulation different from other formulations. The further speciality of the formulation is the strong satisfaction of the cross-sectional constitutive conditions at collocation points. In order to avoid the nested integrations, a special algorithm for the numerical integration over the length of the finite element is proposed. The midpoint scheme is used for the time integration. The performance of the formulation is illustrated via numerical examples, including a stiff multibody system.

1. Introduction

Beam is one of the basic components of the multibody mechanisms and engineering structures. For various reasons beams are often highly flexible, which requires the geometrically nonlinear dynamic theory to be considered in the analysis. A number of geometrically nonlinear dynamic finite-element formulations have been proposed (see, e.g. Refs. [1–16]), which seem to be sufficiently accurate and efficient for practical purposes. These finite-element formulations employ displacements and rotations [3,4,7,8,11,14–16] or absolute nodal coordinates [5,6,10,12,13] as the basic interpolated variables.

The present formulation, though, employs strains. The strain-based finite elements seem to be a promising alternative. They have recently been applied in the geometrically and materially nonlinear static analysis of planar and spatial reinforced concrete structures [17–19] and in the analysis of slip in composite beams [20,21]; there, they have proved to be accurate and robust, exhibiting no locking and demonstrating ability to consider the strain localization in a natural way. The first attempt to apply strain-based elements to dynamics was made by Gams et al. [22]. Their formulation was limited to the constant interpolation of strains. When compared to the displacement-based formulation, the strain-based one is more complex with regard to both theory and computer implementation.

In this paper we present an improved family of strain-based finite elements, which represents a substantial generalization of the results presented in Ref. [22]. The improvements are made regarding (i) the order of

*Corresponding author. Tel.: +386 1 47 68 613; fax: +386 1 47 68 629.
E-mail address: msaje@fgg.uni-lj.si (M. Saje).

0022-460X/$ - see front matter © 2007 Elsevier Ltd. All rights reserved.
doi:10.1016/j.jsv.2007.03.055

interpolation of strains, which is now arbitrary, (ii) the discretization method, which is here the collocation in contrast to the Galerkin method used in Ref. [22], and (iii) the implementation, which now avoids the nested numerical integrations.

2. Kinematic equations

We consider an initially straight planar elastic beam element of initial length L in the (X, Z)-plane of a spatial Cartesian coordinate system (X, Y, Z). We assume that the centroid axis of the beam is parallel to the X-axis in the undeformed state. The shape of the cross-section is assumed constant and symmetric with respect to the plane of deformation. The position of a cross-section relative to the beam axis is identified by the material coordinate $x \in [0, L]$. Reissner's beam theory [23] is employed. It assumes the Bernoulli hypothesis of planar and undistorted cross-sections and considers finite displacements, rotations, membrane, shear and bending strains. Along its centroid axis the beam is subjected to time dependent distributed loads $p_X(x,t)$, $p_Z(x,t)$ and moment $m_Y(x,t)$ (measured per unit length of undeformed axis; t denotes time), and generalized point loads $S_k(t)$ $(k = 1, 2, \ldots, 6)$ at its ends $x = 0$ and L. Loads are assumed to be deformation-independent. For further details the reader may consult, e.g. Refs. [23,24].

The components of the displacement vector, $\mathbf{u}$, of an arbitrary point, x, on the centroid axis in the X- and Z-directions are denoted by $u(x,t)$ and $w(x,t)$, respectively. The relations between the displacement components and the strains were derived by Reissner [23] and read

$$1 + u' - (1+\varepsilon)\cos\varphi - \gamma\sin\varphi = 0, \tag{1}$$

$$w' + (1+\varepsilon)\sin\varphi - \gamma\cos\varphi = 0, \tag{2}$$

$$\varphi' - \kappa = 0. \tag{3}$$

In Eqs. (1)–(3) the prime $(')$ denotes the derivative with respect to x, whereas functions $\varepsilon(x,t)$, $\gamma(x,t)$ and $\kappa(x,t)$ denote the extensional strain, the shear strain (due to the rotation of the cross-section relative to the normal to the deformed axis at x), and the bending strain (the pseudocurvature [26]) of the centroid axis, respectively, while $\varphi(x,t)$ is the rotation of the cross-section at x.

3. Equations of motion

The equations of motion of the beam will be derived from Hamilton's principle [25], which says that the following variation is zero:

$$\delta \int_{t_1}^{t_2} (E_p - E_k)\,\mathrm{d}t = 0 \tag{4}$$

for any kinematically admissible variations of displacements, provided that the variations of displacements vanish at t_1 and t_2. In Eq. (4) and throughout the text, δ denotes the variation. E_p and E_k are potential and kinetic energies, respectively. t_1 is the lower and t_2 the upper boundary of the time interval over which the dynamic equilibrium is satisfied. The kinetic energy of the beam is given by the expression

$$E_k = \frac{1}{2}\int_0^L \rho A \dot{u}^2\,\mathrm{d}x + \frac{1}{2}\int_0^L \rho A \dot{w}^2\,\mathrm{d}x + \frac{1}{2}\int_0^L \rho I_y \dot{\varphi}^2\,\mathrm{d}x, \tag{5}$$

where ρ denotes density of material, A is the area and I_y the centroidal moment of inertia of the cross-section about its y-axis. The superposed dot denotes the time derivative. The potential energy of the elastic beam is

$$\begin{aligned} E_p = {} & \frac{1}{2}\int_0^L EA\varepsilon^2\,\mathrm{d}x + \frac{1}{2}\int_0^L GA_s\gamma^2\,\mathrm{d}x + \frac{1}{2}\int_0^L EI_y\kappa^2\,\mathrm{d}x \\ & - \int_0^L p_X u\,\mathrm{d}x - \int_0^L p_Z w\,\mathrm{d}x - \int_0^L m_Y\varphi\,\mathrm{d}x - \sum_{i=1}^{6} S_i U_i. \end{aligned} \tag{6}$$

E is Young's modulus and G shear modulus of material; A_s is the shear area of the cross-section. U_i ($i = 1, 2, \ldots, 6$) are the generalized boundary displacements at $x = 0$ and L; they are energy complements to the generalized boundary forces S_i (for further details see Refs. [24,27–29]).

Eqs. (1)–(3) represent three constraining conditions for six functions $u(x,t)$, $w(x,t)$, $\varphi(x,t)$, $\varepsilon(x,t)$, $\gamma(x,t)$ and $\kappa(x,t)$. Following the methodology inspired by the Lagrangian multipliers method in constrained problems of calculus of variation, three independent Lagrangian multipliers $\mathscr{R}_X$, $\mathscr{R}_Z$ and $\mathscr{M}$ are introduced, by which the constraints (1)–(3) are multiplied and then integrated over the length of the beam. Adding the resulting equations to the functional in Eq. (4) yields the augmented Hamilton principle

$$\delta \int_{t_1}^{t_2} \left(E_p - E_k + \int_0^L \mathscr{R}_X(1 + u' - (1+\varepsilon)\cos\varphi - \gamma\sin\varphi)\,\mathrm{d}x + \int_0^L \mathscr{R}_Z(w' + (1+\varepsilon)\sin\varphi - \gamma\cos\varphi)\,\mathrm{d}x + \int_0^L \mathscr{M}(\varphi' - \kappa)\,\mathrm{d}x \right) \mathrm{d}t = 0. \tag{7}$$

Eq. (7) requires the variation of a number of terms. Only the variation of the kinetic energy is worked out here [27]:

$$\begin{aligned} \delta \int_{t_1}^{t_2} E_k\,\mathrm{d}t &= \int_{t_1}^{t_2} \left(\int_0^L \rho A \ddot{u}\delta\dot{u}\,\mathrm{d}x + \int_0^L \rho A \ddot{w}\delta\dot{w}\,\mathrm{d}x + \int_0^L \rho I_y \ddot{\varphi}\delta\dot{\varphi}\,\mathrm{d}x \right) \mathrm{d}t \\ &= \int_0^L (\rho A \dot{u}\delta u + \rho A \dot{w}\delta w + \rho I_y \dot{\varphi}\delta\varphi)|_{t_1}^{t_2}\,\mathrm{d}x \\ &\quad - \int_{t_1}^{t_2} \left(\int_0^L \rho A \ddot{u}\delta u\,\mathrm{d}x + \int_0^L \rho A \ddot{w}\delta w\,\mathrm{d}x + \int_0^L \rho I_y \ddot{\varphi}\delta\varphi\,\mathrm{d}x \right) \mathrm{d}t. \end{aligned}$$

As the first variations δu, δw and $\delta\varphi$ must vanish at t_1 and t_2, we have

$$\delta \int_{t_1}^{t_2} E_k\,\mathrm{d}t = -\int_{t_1}^{t_2} \left(\int_0^L \rho A \ddot{u}\delta u\,\mathrm{d}x + \int_0^L \rho A \ddot{w}\delta w\,\mathrm{d}x + \int_0^L \rho I_y \ddot{\varphi}\delta\varphi\,\mathrm{d}x \right) \mathrm{d}t. \tag{8}$$

After Eq. (7) has been varied, and the terms $\mathscr{R}_X\delta u'$, $\mathscr{R}_Z\delta w'$ and $\mathscr{M}\delta\varphi'$ integrated by parts and rearranged, we obtain

$$\begin{aligned} &\int_0^L (EA\varepsilon - \mathscr{N})\delta\varepsilon\,\mathrm{d}x + \int_0^L (GA_s\gamma - \mathscr{Q})\delta\gamma\,\mathrm{d}x + \int_0^L (EI_y\kappa - \mathscr{M})\delta\kappa\,\mathrm{d}x \\ &+ \int_0^L (\mathscr{R}'_X + p_X - \rho A\ddot{u})\delta u\,\mathrm{d}x + \int_0^L (\mathscr{R}'_Z + p_Z - \rho A\ddot{w})\delta w\,\mathrm{d}x \\ &+ \int_0^L (\mathscr{M}' - (1+\varepsilon)\mathscr{Q} + \gamma\mathscr{N} + m_Y - \rho I_y\ddot{\varphi})\delta\varphi\,\mathrm{d}x \\ &+ \int_0^L (1 + u' - (1+\varepsilon)\cos\varphi - \gamma\sin\varphi)\delta\mathscr{R}_X\,\mathrm{d}x \\ &- \int_0^L (w' + (1+\varepsilon)\sin\varphi - \gamma\cos\varphi)\delta\mathscr{R}_Z\,\mathrm{d}x + \int_0^L (\varphi' - \kappa)\delta\mathscr{M}\,\mathrm{d}x \\ &- (S_1 + \mathscr{R}_X(0))\delta U_1 - (S_2 + \mathscr{R}_Z(0))\delta U_2 - (S_3 + \mathscr{M}(0))\delta U_3 \\ &- (S_4 - \mathscr{R}_X(L))\delta U_4 - (S_5 - \mathscr{R}_Z(L))\delta U_5 - (S_6 - \mathscr{M}(L))\delta U_6 = 0. \end{aligned} \tag{9}$$

In Eq. (9) variations $\delta\varepsilon$, $\delta\gamma$, $\delta\kappa$, δu, δw, $\delta\varphi$, $\delta\mathscr{R}_X$, $\delta\mathscr{R}_Z$ and $\delta\mathscr{M}$ are independent arbitrary functions of x, and variations δU_1, δU_2, δU_3, δU_4, δU_5 and δU_6 are independent arbitrary parameters, provided that the variation is zero if the corresponding nodal displacement U_i is prescribed. According to the fundamental lemma of calculus of variation, the coefficients of the independent variations should vanish identically for

Eq. (9) to be satisfied for arbitrary variations. The following equations of motion of the beam are obtained for any $t \geqslant 0$:

Constitutive equations, $x \in [0, L]$:

$$EA\varepsilon - \mathscr{N} = 0, \tag{10}$$

$$GA_s\gamma - \mathscr{Q} = 0, \tag{11}$$

$$EI_y\kappa - \mathscr{M} = 0. \tag{12}$$

Kinematic equations, $x \in (0, L)$:

$$1 + u' - (1 + \varepsilon)\cos\varphi - \gamma\sin\varphi = 0, \tag{13}$$

$$w' + (1 + \varepsilon)\sin\varphi - \gamma\cos\varphi = 0, \tag{14}$$

$$\varphi' - \kappa = 0. \tag{15}$$

Equations of motion, $x \in (0, L)$:

$$\mathscr{R}'_X + p_X - \rho A\ddot{u} = 0, \tag{16}$$

$$\mathscr{R}'_Z + p_Z - \rho A\ddot{w} = 0, \tag{17}$$

$$\mathscr{M}' - (1 + \varepsilon)\mathscr{Q} + \gamma\mathscr{N} + m_Y - \rho I_y\ddot{\varphi} = 0. \tag{18}$$

The natural and essential boundary conditions corresponding to Eqs. (10)–(18) are:

$$x = 0 : S_1 + \mathscr{R}_X(0) = 0 \quad \text{or } u(0) = U_1, \tag{19}$$

$$S_2 + \mathscr{R}_Z(0) = 0 \quad \text{or } w(0) = U_2, \tag{20}$$

$$S_3 + \mathscr{M}(0) = 0 \quad \text{or } \varphi(0) = U_3, \tag{21}$$

$$x = L : S_4 - \mathscr{R}_X(L) = 0 \quad \text{or } u(L) = U_4, \tag{22}$$

$$S_5 - \mathscr{R}_Z(L) = 0 \quad \text{or } w(L) = U_5, \tag{23}$$

$$S_6 - \mathscr{M}(L) = 0 \quad \text{or } \varphi(L) = U_6. \tag{24}$$

Eqs. (10)–(18) constitute the system of nine equations for nine unknown functions $\varepsilon(x, t)$, $\gamma(x, t)$, $\kappa(x, t)$, $u(x, t)$, $w(x, t)$, $\varphi(x, t)$, $\mathscr{R}_X(x, t)$, $\mathscr{R}_Z(x, t)$ and $\mathscr{M}(x, t)$ along with the natural and essential boundary conditions (19)–(24).

From Eqs. (16)–(18) it is clear that the Lagrangian multipliers $\mathscr{R}_X$ and $\mathscr{R}_Z$ represent axial and shear forces with respect to the spatial coordinate system

$$\mathscr{N} = \mathscr{R}_X\cos\varphi - \mathscr{R}_Z\sin\varphi, \tag{25}$$

$$\mathscr{Q} = \mathscr{R}_X\sin\varphi + \mathscr{R}_Z\cos\varphi, \tag{26}$$

while $\mathscr{M}$ is the bending moment. In order to minimize the number of unknown functions in our final discretized system of equations, some of these equations are integrated separately. The integration of kinematic equations (13)–(15) with respect to x gives the displacements and the rotation at x in terms of the deformation variables, ε, γ and κ:

$$u(x, t) = u(0, t) + \int_0^x ((1 + \varepsilon)\cos\varphi + \gamma\sin\varphi)\,\mathrm{d}\xi - x, \tag{27}$$

$$w(x, t) = w(0, t) - \int_0^x ((1 + \varepsilon)\sin\varphi - \gamma\cos\varphi)\,\mathrm{d}\xi, \tag{28}$$

$$\varphi(x, t) = \varphi(0, t) + \int_0^x \kappa\,\mathrm{d}\xi. \tag{29}$$

While $u(0, t) = U_1(t)$, $w(0, t) = U_2(t)$, $\varphi(0, t) = U_3(t)$ can meet any given essential boundary conditions at $x = 0$, parameters $u(L, t)$, $w(L, t)$, $\varphi(L, t)$ do not automatically satisfy the conditions at $x = L$, unless strains ε,

γ and κ are chosen exactly as needed. Consequently, one must explicitly require that ε, γ and κ be such that for any time t

$$u(L,t) = u(0,t) + \int_0^L ((1+\varepsilon)\cos\varphi + \gamma\sin\varphi)\,\mathrm{d}x - L = U_4(t), \tag{30}$$

$$w(L,t) = w(0,t) - \int_0^L ((1+\varepsilon)\sin\varphi - \gamma\cos\varphi)\,\mathrm{d}x = U_5(t), \tag{31}$$

$$\varphi(L,t) = \varphi(0,t) + \int_0^L \kappa\,\mathrm{d}x = U_6(t). \tag{32}$$

The relations between the Lagrangian multipliers $\mathscr{R}_X$, $\mathscr{R}_Z$ and $\mathscr{M}$ and the strains ε, γ and κ are obtained by the integration of Eqs. (16)–(18):

$$\mathscr{R}_X(x,t) = \mathscr{R}_X(0,t) - \int_0^x (p_X - \rho A\ddot{u})\,\mathrm{d}\xi, \tag{33}$$

$$\mathscr{R}_Z(x,t) = \mathscr{R}_Z(0,t) - \int_0^x (p_Z - \rho A\ddot{w})\,\mathrm{d}\xi, \tag{34}$$

$$\mathscr{M}(x,t) = \mathscr{M}(0,t) + \int_0^x ((1+\varepsilon)\mathscr{Q} - \gamma\mathscr{N} - m_Y + \rho I_y\ddot{\varphi})\,\mathrm{d}\xi. \tag{35}$$

It is clear that $\mathscr{R}_X(L,t)$, $\mathscr{R}_Z(L,t)$ and $\mathscr{M}(L,t)$ depend on strains. If they are to meet the prescribed natural boundary conditions at $x = L$, the following equations must be satisfied:

$$\mathscr{R}_X(L,t) = \mathscr{R}_X(0,t) - \int_0^L (p_X - \rho A\ddot{u})\,\mathrm{d}x = S_4(t), \tag{36}$$

$$\mathscr{R}_Z(L,t) = \mathscr{R}_Z(0,t) - \int_0^L (p_Z - \rho A\ddot{w})\,\mathrm{d}x = S_5(t), \tag{37}$$

$$\mathscr{M}(L,t) = \mathscr{M}(0,t) + \int_0^L ((1+\varepsilon)\mathscr{Q} - \gamma\mathscr{N} - m_Y + \rho I_y\ddot{\varphi})\,\mathrm{d}x = S_6(t). \tag{38}$$

Next we claim that Eqs. (27)–(29) and (33)–(35) are satisfied. Consequently, also Eqs. (13)–(15) and (16)–(18)) are satisfied. Thus, $\mathscr{R}_X(L,t)$, $\mathscr{R}_Z(L,t)$ and $\mathscr{M}(L,t)$ can be expressed by $\mathscr{R}_X(0,t)$, $\mathscr{R}_Z(0,t)$, $\mathscr{M}(0,t)$ and the strains using Eqs. (36)–(38). The remaining set of the equations of the beam, Eqs. (10)–(12), (19)–(24) and (30)–(32), then constitute the set of twelve equations for twelve unknowns, i.e. three constitutive equations, six boundary conditions and three kinematic constraints for the determination of three unknown functions of x and t, i.e. $\varepsilon(x,t)$, $\gamma(x,t)$ and $\kappa(x,t)$ and nine time-dependent parameters ($u(0,t)$, $w(0,t)$, $\varphi(0,t)$, $u(L,t)$, $w(L,t)$, $\varphi(L,t)$, $\mathscr{R}_X(0,t)$, $\mathscr{R}_Z(0,t)$, $\mathscr{M}(0,t)$). These equations are supplemented by an appropriate set of initial conditions at $t = 0$.

4. Finite-element formulation

The Lagrangian polynomials, $P_i(x)$ $(i = 1,2,\ldots,N)$, of degree $N-1$ are employed for the spatial approximation of the unknown functions $\varepsilon(x,t)$, $\gamma(x,t)$ and $\kappa(x,t)$ and their variations. Interpolation points are assumed to be distributed regularly over the beam length, $x_i = (i-1)[L/(N-1)]$ $(i = 1,2,\ldots,N)$:

$$\varepsilon(x,t) = \sum_{i=1}^{N} P_i(x)\varepsilon_i(t) \to \delta\varepsilon(x) = \sum_{i=1}^{N} P_i(x)\delta\varepsilon_i(t), \tag{39}$$

$$\gamma(x,t)=\sum_{i=1}^{N}P_i(x)\gamma_i(t)\rightarrow\delta\gamma(x)=\sum_{i=1}^{N}P_i(x)\delta\gamma_i(t), \tag{40}$$

$$\kappa(x,t)=\sum_{i=1}^{N}P_i(x)\kappa_i(t)\rightarrow\delta\kappa(x)=\sum_{i=1}^{N}P_i(x)\delta\kappa_i(t). \tag{41}$$

Once the nodal values ε_i, γ_i and κ_i at a given time t_n are known, the remaining quantities can easily be determined. Since the terms to be encountered involve integrals, which cannot be analytically integrated for higher-order polynomials, one is forced to use the numerical integration. For higher-order interpolations this represents a computationally demanding task, because the nested integrals of depth up to five have to be evaluated in some terms of the tangent stiffness matrix, which renders the calculations slow and computer memory demanding. Let us give an example. Assume that we need the value of the multiplier $\mathscr{R}_X$ at a given point x. After inserting $u(x,t)$ from Eq. (27) into Eq. (33), we have

$$\begin{aligned}\mathscr{R}_X(x,t)&=\mathscr{R}_X(0,t)-\int_0^x(p_X-\rho A\ddot{u})\,\mathrm{d}\xi\\&=\mathscr{R}_X(0,t)-\int_0^x(p_X-\rho A\ddot{u}(0,t))\,\mathrm{d}\xi\\&\quad+\int_0^x\rho A\int_0^\xi\frac{\mathrm{d}^2}{\mathrm{d}t^2}((1+\varepsilon)\cos\varphi+\gamma\sin\varphi)\,\mathrm{d}\eta\,\mathrm{d}\xi.\end{aligned} \tag{42}$$

The Gaussian integration of the double integral in Eq. (42) requires a nested algorithm: for each Gaussian point of the external numerical integration, a complete evaluation of the internal integral up to the Gaussian point is required. Hence the number of the numerical operations increases with N^2+N compared to N needed in a single integral. $\mathscr{R}_X$ is needed both in the residual vector and the stiffness matrix integrations; this requires the third numerical integration in a row. Hence, these nested integrations become computationally very demanding. An alternative is proposed here, which elegantly avoids these inconveniences.

The key idea of a numerical integration is to choose a set of K independent functions $P_i(\xi)$ to approximate the integrand, $f(\xi)$, $\xi\in[-1,1]$, in the form of a linear combination

$$f(\xi)=\sum_{i=1}^{K}f(\xi_i)P_i(\xi), \tag{43}$$

with ξ_i being the abscissae of the points of interpolation. After the approximation (43) is inserted into the integral and the integration performed over the domain $[-1,1]$, we have

$$\int_{-1}^{1}f(\xi)\mathrm{d}\xi=\sum_{i=1}^{K}w_if(\xi_i), \tag{44}$$

with $w_i=\int_{-1}^{1}P_i(\xi)\,\mathrm{d}\xi$ denoting the weights of the integration.

The same idea is followed in the present paper. In order to integrate numerically the integrals involved in our formulation, we first have to interpolate their integrands. The implementation is, however, done in a specific way, as explained in the sequel. For example, to obtain the displacements by the integration of Eqs. (27) and (28), we interpolate the spatial derivatives of displacements $u'(x,t)$, $w'(x,t)$ in the following way:

$$u'(x,t)=\sum_{i=1}^{N}P_i(x)a_i(t), \tag{45}$$

$$w'(x,t)=\sum_{i=1}^{N}P_i(x)b_i(t), \tag{46}$$

with a_i and b_i ($i = 1, 2, \ldots, N$) being expressed by the nodal variables (ε_i, γ_i, κ_i) through kinematic Eqs. (1) and (2):

$$a_i = (1 + \varepsilon_i)\cos\varphi_i + \gamma_i \sin\varphi_i - 1, \tag{47}$$

$$b_i = -(1 + \varepsilon_i)\sin\varphi_i + \gamma_i \cos\varphi_i. \tag{48}$$

$P_i(\xi)$ are taken to be the Lagrangian polynomials ($i = 1, 2, 3, \ldots, N$). Integrating Eqs. (45) and (46) with respect to x gives displacements $u(x, t)$ and $w(x, t)$:

$$u(x, t) = u(0, t) + \sum_{i=1}^{N} IP_i(x) a_i(t), \tag{49}$$

$$w(x, t) = w(0, t) + \sum_{i=1}^{N} IP_i(x) b_i(t). \tag{50}$$

Here $IP_i(x) = \int_0^x P_i(\xi)\,\mathrm{d}\xi$ is the analytical integral of the Lagrangian polynomial $P_i(x)$. Rotation $\varphi(x, t)$ is obtained by the direct integration of Eq. (3) in combination with Eq. (41):

$$\varphi(x, t) = \varphi(0, t) + \int_0^x \kappa(\xi, t)\,\mathrm{d}\xi = \varphi(0, t) + \sum_{i=1}^{N} IP_i(x)\kappa_i(t). \tag{51}$$

The idea of interpolating derivatives rather than directly numerically integrating the integrand is also followed for $\mathscr{M}$. Hence

$$\mathscr{M}'(x, t) = \sum_{i=1}^{N} P_i(x) c_i(t), \tag{52}$$

with c_i ($i = 1, 2, \ldots, N$) following from Eq. (18):

$$c_i = (1 + \varepsilon_i)\mathscr{Q}_i - \gamma_i \mathscr{N}_i - m_{Yi} + \rho I_y \ddot{\varphi}_i. \tag{53}$$

Integrating Eq. (52) with respect to x gives $\mathscr{M}(x, t)$:

$$\mathscr{M}(x, t) = \mathscr{M}(0, t) + \sum_{i=1}^{N} IP_i(x) c_i(t). \tag{54}$$

The need for the integration other than that of the Lagrangian polynomials is completely eliminated. This integration can be performed analytically once for all, which makes the integration computationally very effective.

The interpolations introduced in Eqs. (45), (46) and (52) should be regarded as a part of the numerical integration method, and not as the interpolation in the sense of the finite-element method.

The second time derivatives of u, w, φ are obtained by the differentiation of Eqs. (49)–(51)

$$\ddot{u}(x, t) = \ddot{u}(0, t) + \sum_{i=1}^{N} IP_i(x) \ddot{a}_i(t), \tag{55}$$

$$\ddot{w}(x, t) = \ddot{w}(0, t) + \sum_{i=1}^{N} IP_i(x) \ddot{b}_i(t), \tag{56}$$

$$\ddot{\varphi}(x, t) = \ddot{\varphi}(0, t) + \sum_{i=1}^{N} IP_i(x) \ddot{\kappa}_i(t). \tag{57}$$

Their spatial integrals are needed for calculating $\mathscr{R}_X(x,t)$, $\mathscr{R}_Z(x,t)$ and $\mathscr{M}(x,t)$ and are dealt with in the following way:

$$\int_0^x \ddot{u}(\xi,t)\,\mathrm{d}\xi = \ddot{u}(0,t)x + \sum_{i=1}^{N} IIP_i(x)\ddot{a}_i(t), \tag{58}$$

$$\int_0^x \ddot{w}(\xi,t)\,\mathrm{d}\xi = \ddot{w}(0,t)x + \sum_{i=1}^{N} IIP_i(x)\ \ddot{b}_i(t), \tag{59}$$

$$\int_0^x \ddot{\varphi}(\xi,t)\,\mathrm{d}\xi = \ddot{\varphi}(0,t)x + \sum_{i=1}^{N} IIP_i(x)\ddot{\kappa}_i(t), \tag{60}$$

where $IIP_i(x) = \int_0^x \int_0^\xi P_i(\eta)\,\mathrm{d}\eta\,\mathrm{d}\xi$. The time derivatives $\ddot{a}_i$ and $\ddot{b}_i$ are obtained in terms of ε_i, γ_i and κ_i and their time derivatives obtained by the differentiation of Eqs. (47)–(48).

Our finite-element formulation is based on the collocation-type of the spatial discretization [19,26] rather than on the standard Galerkin-type. We assume that the collocation and the interpolation points coincide, so that the points are regularly distributed over the beam length, $x_i = (i-1)[L/(N-1)]$. Eqs. (10)–(12), (19)–(24) and (30)–(32) yield the following system of semi-discrete equations of motion of the beam finite element:

$$g_i = EA\varepsilon_i(t) - \mathscr{N}_i(t) = 0, \quad i = 1,\ldots,N \tag{61}$$

$$g_{N+i} = GA_s\gamma_i(t) - \mathscr{Q}_i(t) = 0, \quad i = 1,\ldots,N \tag{62}$$

$$g_{2N+i} = EI_y\kappa_i(t) - \mathscr{M}_i(t) = 0, \quad i = 1,\ldots,N \tag{63}$$

$$g_{3N+1} = u(L,t) - u_N(t) = 0, \tag{64}$$

$$g_{3N+2} = w(L,t) - w_N(t) = 0, \tag{65}$$

$$g_{3N+3} = \varphi(L,t) - \varphi_N(t) = 0, \tag{66}$$

$$g_{3N+4} = S_1(t) + \mathscr{R}_X(0,t) = 0, \tag{67}$$

$$g_{3N+5} = S_2(t) + \mathscr{R}_Z(0,t) = 0, \tag{68}$$

$$g_{3N+6} = S_3(t) + \mathscr{M}(0,t) = 0, \tag{69}$$

$$g_{3N+7} = S_4(t) - \mathscr{R}_{XN}(t) = 0, \tag{70}$$

$$g_{3N+8} = S_5(t) - \mathscr{R}_{ZN}(t) = 0, \tag{71}$$

$$g_{3N+9} = S_6(t) - \mathscr{M}_N(t) = 0. \tag{72}$$

$u_N, w_N, \varphi_N, \mathscr{R}_{XN}, \mathscr{R}_{ZN}$ and $\mathscr{M}_N$ denote the values of the variables at the end point $i = N$. Eqs. (61)–(72) constitute a system of $3N+9$ algebraic-differential equations for $3N+9$ unknown functions of time: $\varepsilon_i(t)$, $\gamma_i(t)$, $\kappa_i(t)$ $(i = 1,2,\ldots,N)$, $u(0,t)$, $w(0,t)$, $\varphi(0,t)$, $u(L,t)$, $w(L,t)$, $\varphi(L,t)$, $\mathscr{R}_X(0,t)$, $\mathscr{R}_Z(0,t)$ and $\mathscr{M}(0,t)$. Eqs. (64)–(69) are algebraic, and Eqs. (61)–(63) and (70)–(72) are differential equations in time of the second order. Observe that this system has an implicit form $\mathscr{F}(\mathbf{u},\dot{\mathbf{u}},\ddot{\mathbf{u}},t) = \mathbf{0}$ and thus does not comply with the standard form $\mathbf{M}\ddot{\mathbf{u}} + \mathbf{P}(\mathbf{u}) = \mathbf{F}$ used, e.g. in Ref. [14]. The constitutive equations (61)–(63) represent the so called consistency conditions [26,28], which impose the equality of the cross-sectional constitutive and equilibrium forces. The satisfaction of the consistency conditions in a point-wise manner can increase the accuracy of internal forces in materially nonlinear problems. Observe that the consistency conditions are not strongly satisfied in standard displacement-based formulations.

The internal degrees of freedom, i.e. $\mathscr{R}_X(0,t)$, $\mathscr{R}_Z(0,t)$, $\mathscr{M}(0,t)$, and the internal nodal strains, $\varepsilon_j(t)$, $\gamma_j(t)$, $\kappa_j(t)$ $(j = 1,2,\ldots,N)$, are eliminated prior to assembling the equations of motion of the structure. This leaves

us only with boundary displacements and rotations of each element, and a fairly small tangent stiffness matrix of the entire structure. Introducing any kind of joints in such a formulation presents no extra complexity, as the desired degrees of freedom are condensed out in the same way as the internal nodal strains or forces.

In the present formulation, only the Lagrangian polynomials of a given degree need to be integrated, and this integration can be prepared in advance. Thus, the order of the numerical integration becomes irrelevant. This differs from standard displacement-based formulations, where the order of the numerical integration (full, reduced or selectively reduced) plays a crucial role in alleviating locking.

5. Time integration

In the present article we use the 'midpoint' implicit time integration scheme [25]. Introducing ψ as a generic symbol of the discrete unknown functions of time ε_i, γ_i, κ_i $(i = 1, 2, \ldots, N)$, $u(0)$, $w(0)$, $\varphi(0)$, $u(L)$, $w(L)$, $\varphi(L)$, $\mathscr{R}_X(0)$, $\mathscr{R}_Z(0)$ and $\mathscr{M}(0)$, we have the following midpoint rule approximations for the midpoint values of ψ and its time derivatives:

$$\psi_{n+\frac{1}{2}} = \tfrac{1}{2}(\psi_n + \psi_{n+1}), \tag{73}$$

$$\dot{\psi}_{n+\frac{1}{2}} = \frac{\psi_{n+1} - \psi_n}{\Delta t}, \tag{74}$$

$$\ddot{\psi}_{n+\frac{1}{2}} = \frac{2}{\Delta t^2}(\psi_{n+1} - \psi_n - \Delta t\dot{\psi}_n). \tag{75}$$

Subscript n denotes the converged value at t_n with the known solutions ψ_n and $\dot{\psi}_n$, while $n+1$ denotes the unknown function value ψ_{n+1} at time $t_n + \Delta t$; Δt denotes the time increment. Subscript $n + 1/2$ refers to the midpoint time ($t_{n+1/2} = t_n + (\Delta t/2)$). Once the nodal values of the unknowns, ψ_{n+1}, have been obtained, their velocity and acceleration updates at t_{n+1} are given by:

$$\dot{\psi}_{n+1} = \frac{2}{\Delta t}\left(\psi_{n+1} - \psi_n - \frac{\Delta t}{2}\dot{\psi}_n\right), \tag{76}$$

$$\ddot{\psi}_{n+1} = \frac{4}{\Delta t^2}\left(\psi_{n+1} - \psi_n - \Delta t\dot{\psi}_n - \frac{\Delta t^2}{4}\ddot{\psi}_n\right). \tag{77}$$

Having the nodal values at $t_{n+1/2}$ and t_{n+1}, we can evaluate the unknowns at any point of the centroid axis from Eqs. (39)–(41) (strains), Eqs. (49)–(51) (displacements and rotation) and Eqs. (55)–(57) (accelerations). The axial and shear forces and the bending moment are obtained directly from the corresponding strains and the constitutive equations. Due to the presence of the algebraic equations, the present system of algebraic-differential equations is stiff by definition. Therefore, the midpoint time integration scheme is not stable if used in a straightforward fashion. In order to improve stability, the algebraic equations, i.e. the kinematic constraints Eqs. (64)–(66), are satisfied at t_{n+1} rather than at $t_{n+1/2}$. Eqs. (61)–(63) and (67)–(72) are taken to be satisfied at the midpoint time, $t_{n+1/2}$, however. This improves stability of the time integration scheme, yet does not make it unconditionally stable.

Inserting Eqs. (73)–(75) into Eqs. (61)–(72) yields the system of nonlinear algebraic equations for nodal values ψ_{n+1}. The system is solved iteratively by the Newton method.

6. Numerical examples

To show the validity of the present formulation and to illustrate its performance, we consider three interesting examples: (i) the oscillation of a cantilever beam, (ii) a free flight of two flexible beams connected by a hinge, and (iii) motion of four flexible beams connected by revolute or translational joints. In the first example, we focus our attention on the comparison with the formulation given in Ref. [22]. This serves to verify the new computational procedure and to demonstrate a substantial reduction of the computational time. Furthermore, the example demonstrates a locking-free behavior of both the previous [22] and the present

strain-based formulations. The second numerical example compares the present formulation with the displacement-based formulation [8], thus verifying the formulation even further, and analyzes possible advantages and disadvantages of the two formulations. The final example is representative for stiff problems [1,2,8,16,25]; it was chosen to show the performance of our strain-based elements in such problems.

6.1. Cantilever beam

In this numerical example we compare the present formulation with the formulation presented in Ref. [22] regarding the accuracy and the computational efficiency. The geometric properties of the cantilever are deliberately chosen in such a way that shear locking would occur [30], if the method of solution utilized the displacement-based Galerkin-type finite elements.

The cantilever in Fig. 1 is loaded by force $F = 250\,\mathrm{N}$, instantaneously applied at $t = 0\,\mathrm{s}$, and remaining constant during the analysis. The cross-section is solid rectangular. If solved by the displacement-based formulation, Rong and Lu [30] showed that the case becomes sensitive to shear locking when $\log_{10}(L/i_y) > 1$ (here $i_y = \sqrt{I_y/A}$). We adopted the following values: $\log_{10}(L/i_y) = 2$, $L = 1\,\mathrm{m}$, the width of the cross-section $b = 0.01\,\mathrm{m}$, the height of the cross-section $h = L\sqrt{12}/10^2 \simeq 0.03464\,\mathrm{m}$. According to Ref. [30], this choice should lock the deflection for the displacement-based elements. The analysis was run up till 0.1 s with the time step $\Delta t = 0.0005\,\mathrm{s}$.

The time variation of the tip deflection is shown in Fig. 1. The results for the tip deflection at two different times, $t = 0.05$ and 0.1 s, along with the maximal deflection, the relative errors with respect to the 360 dof of 20 FE_3 solution and the computational times are for elements of various order (E_i) and various finite element meshes displayed in Table 1 for the present formulation and, in Table 2, for the formulation presented in Ref. [22].

The data in the tables show: (i) both formulations converge to the same results, hence validating the new computational procedure, (ii) as expected, the rate of convergence increases with the order of the element, (iii) good results are obtained with only a few dofs, (iv) locking is absent, and finally (v) computational times are roughly 10-times smaller indicating a dramatically enhanced efficiency of our new formulation.

6.2. A two-body system in free flight

We analyze a two-body system made up of two flexible beams connected by a revolute joint. This case was originally proposed and analyzed by Simo and Vu-Quoc [14]. The system is initially at an inclined position (Fig. 2) and is set into motion by applying a force and a torque at the free end (A) of the lower beam. The applied forces are removed after 0.5 s, leaving the system to continue its motion in free flight. Hsiao and

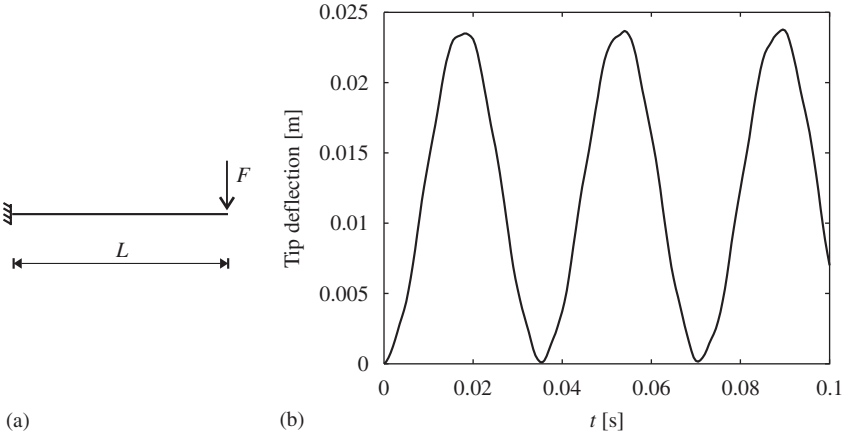

Fig. 1. Cantilever beam: (a) geometry and loading, (b) tip deflection. Material and cross-sectional data: $E = 2 \times 10^{11}\,\mathrm{N/m^2}$, $v = 0.3$, $\rho = 7860\,\mathrm{kg/m^3}$, $b/h = 0.01/0.03464\,\mathrm{m}$.

Table 1
Present formulation

FE	dof	$t = 0.05$ s		$t = 0.1$ s		Max. $w(L)$ (m)	Comp. time (s)[a]
		$w(L)$ (m)	Rel. err.	$w(L)$ (m)	Rel. err.		
1 FE_2	15	0.02296	4.E − 02	0.00397	4.E − 01	0.02405	4.0
1 FE_3	18	0.02168	2.E − 02	0.00790	1.E − 01	0.02400	4.7
1 FE_4	21	0.02212	1.E − 04	0.00708	1.E − 02	0.02360	5.3
2 FE_2	30	0.02177	2.E − 02	0.00687	2.E − 02	0.02404	6.5
2 FE_3	36	0.02214	8.E − 04	0.00697	5.E − 03	0.02368	7.7
2 FE_4	42	0.02216	2.E − 03	0.00700	4.E − 04	0.02372	9.3
4 FE_2	60	0.02208	2.E − 03	0.00705	7.E − 03	0.02382	11.5
4 FE_3	72	0.02213	4.E − 04	0.00700	3.E − 04	0.02375	14.3
4 FE_4	84	0.02212	5.E − 05	0.00700	9.E − 05	0.02377	17.1
20 FE_3	360	0.02212		0.00700		0.02377	64.4

[a]The time interval $[0, 0.1]$ s.

Table 2
The strain-based formulation with the nested integration [22]

FE	dof	$t = 0.05$ s		$t = 0.1$ s		Max. $w(L)$ (m)	Comp. time (s)[a]
		$w(L)$ (m)	Rel. Err.	$w(L)$ (m)	Rel. Err.		
1 FE_0	9	0.00672	7.E − 01	0.01688	1.E + 00	0.01806	23.6
2 FE_0	18	0.02208	2.E − 03	0.00039	9.E − 01	0.02256	41.8
3 FE_0	27	0.02209	1.E − 03	0.00317	5.E − 01	0.02338	60.9
4 FE_0	36	0.02231	9.E − 03	0.00506	3.E − 01	0.02357	77.0
5 FE_0	45	0.02177	2.E − 02	0.00540	2.E − 01	0.02376	98.4
6 FE_0	54	0.02181	1.E − 02	0.00610	1.E − 01	0.02385	115.8
8 FE_0	72	0.02200	5.E − 03	0.00684	2.E − 02	0.02393	148.7
10 FE_0	90	0.02205	3.E − 03	0.00699	3.E − 05	0.02388	176.9
40 FE_0	360	0.02211		0.00699		0.02379	743.0

[a]The time interval $[0, 0.1]$ s.

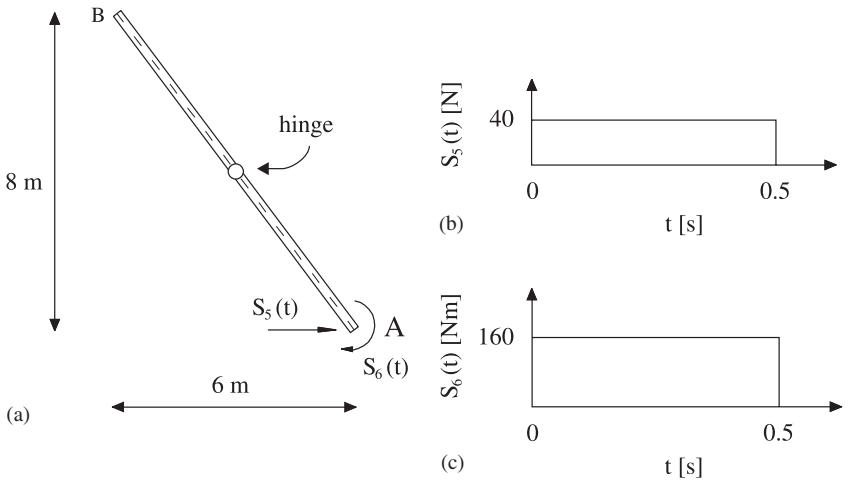

Fig. 2. Two-body system: (a) initial configuration, (b) time variation of force S_5, (c) time variation of torque S_6. Material and cross-sectional data: $EA = GA_s = 1 \times 10^6$ N, $EI_y = 1 \times 10^4$ Nm^2, $\rho A = 1$ kg/m, $\rho I_y = 10$ kg m.

Jang [7] and Iura and Atluri [9] also studied motion of a two-body system in free flight, but used different data: a different value of the moment of inertia of the upper beam and a different removal time (2.5 s in place of 0.5 s employed here and in Ref. [14]). The accuracy check in an iteration step was performed on the basis of the nodal displacement iterative increments, δX, using the criterion

$$\frac{\|\delta X\|}{\max(1, \|X\|)} < 10^{-10}. \tag{78}$$

At all time stations, four Newton's iterations sufficed to reach the tolerance 10^{-10}. This proves that the rate of convergence of the Newton method was quadratic indeed.

The sequence of motion is depicted in Fig. 3. The system undergoes large displacements and rotations, while strains remain relatively small.

For the analysis of the accuracy of the solution, we employed the elements with the quadratic strain interpolation and gradually increased the number of elements. The graphs of the relative error, evaluated relative to the results of the 20-element mesh, $\|\psi_N - \psi_{20}\|/\|\psi_{20}\|$, of displacements at end points A and B as functions of the number of finite elements ($n = 2, 4, 6, 8, 10$) at $t = 10$ s are displayed in Fig. 4.

We now compare the present formulation with the displacement-based formulation by Ibrahimbegović and Mamouri [8]. In order to compare fairly the results of the two formulations, we have made our own computer program based on their energy conserving formulation. We used the reduced integration for the tangent stiffness matrix and the residual vector to alleviate locking, whereas the mass matrix was integrated exactly [14]. In all the analyses, the constant time integration step $\Delta t = 0.1$ s was used.

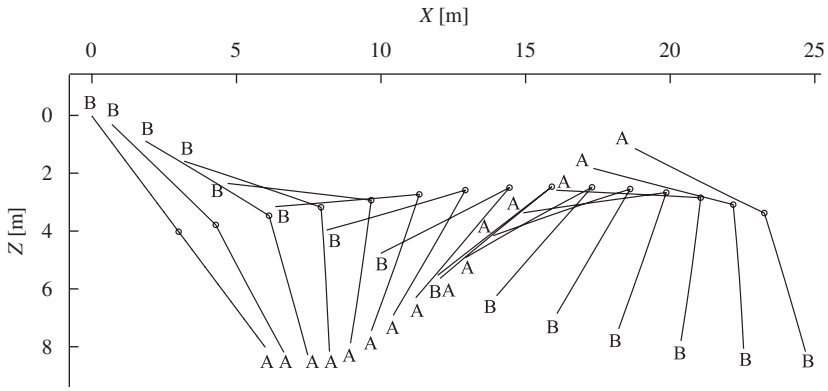

Fig. 3. Motion of the two-body system in time interval [0, 10.5] s. The sequence of motion is depicted in 0.75 s intervals. Time step $\Delta t = 0.05$ s. Two fourth-order strain-based finite elements.

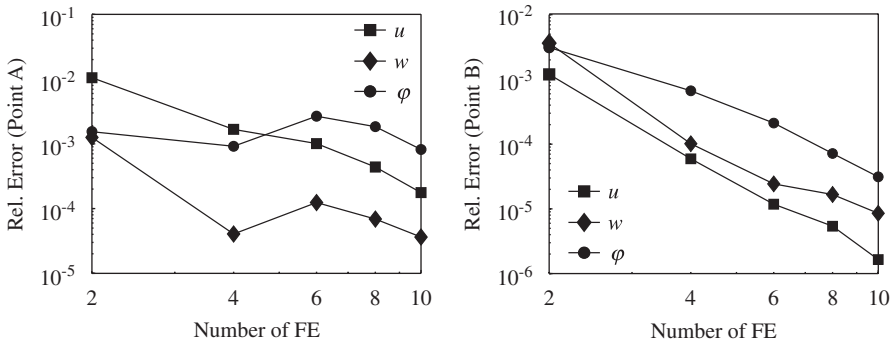

Fig. 4. Motion of the two-body system. Convergence properties at $t = 10$ s. Relative error vs. number of finite elements for point *B*. Square, *u*; diamond, *w*; circle, φ.

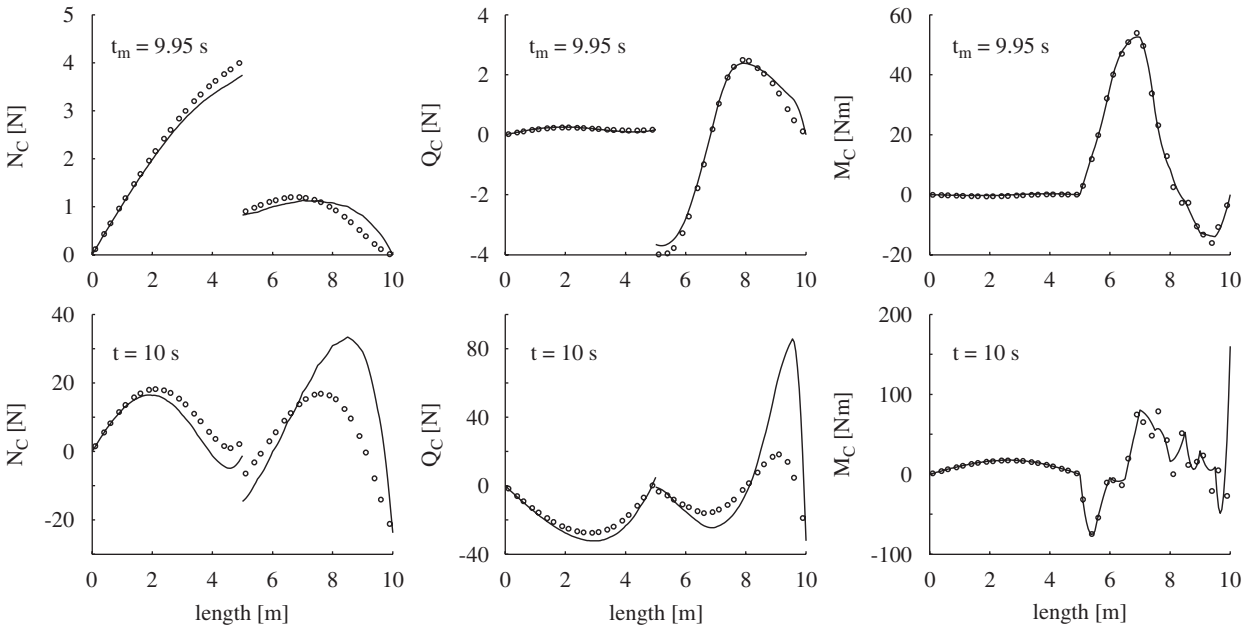

Fig. 5. Motion of the two-body system. Variation of internal forces over length at $t_{n+1/2} = 9.95$ s, top, and at $t_{n+1} = 10$ s, bottom. 20 quadratic elements. Solid line: present formulation, circles: displacement-based formulation [8].

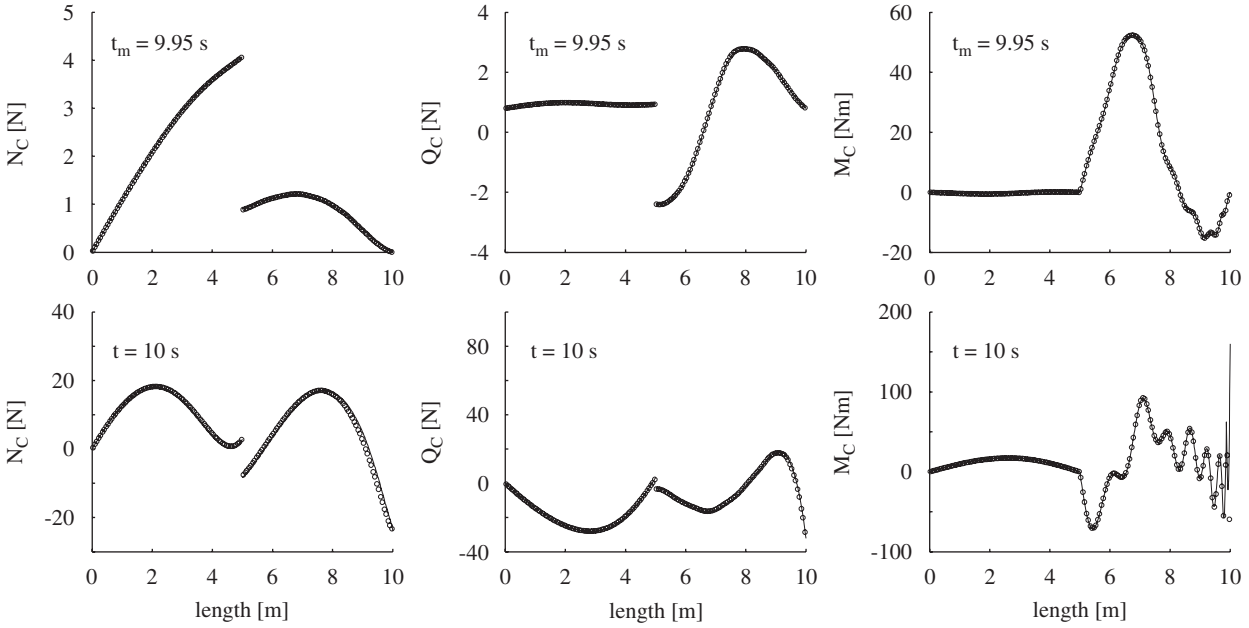

Fig. 6. Motion of the two-body system. Variation of internal forces over length at $t_{n+1/2} = 9.95$ s, top, and at $t_{n+1} = 10$ s, bottom. 80 quadratic elements. Solid line: present formulation, circles: displacement-based formulation [8].

Figs. 5 and 6 compare the variations of internal forces over the length of the system, if they are calculated directly from the constitutive equations. For the displacement-based formulation, the internal forces were evaluated only at two Gaussian points of an element and the values marked with circles. For the strain-based formulation, the values were obtained at 10 regularly distributed points and the variation marked by an

interpolating solid line. Fig. 5 depicts the variations at $t_{n+1/2} = 9.95\,\text{s}$ and $t_{n+1} = 10\,\text{s}$ for the 20-element mesh, and Fig. 6 for the 80-element mesh. The midpoint values of the internal forces were taken as the average values of the internal forces at times t_n and t_{n+1}. Some differences in values are observed at time $t_{n+1} = 10\,\text{s}$ between the displacement-based and the present formulation for the 20-element mesh. The differences, however, vanish for the 80-element mesh, see Fig. 6.

The comparison of the results in Figs. 5 and 6 at $t_{n+1} = 10\,\text{s}$ shows that the internal forces obtained by the displacement-based formulation on the 20-element mesh practically coincide with those for the 80-element mesh. Thus, the internal forces at $t_{n+1} = 10\,\text{s}$ seem to be better described by the displacement-based formulation. The differences, however, appear to be much smaller, if the comparison is made at the midpoint time $t_{n+1/2} = 9.95\,\text{s}$.

6.3. Motion of a four-body system

This case is adopted from Ibrahimbegović and Mamouri [8]. The initial geometry of the system along with material properties of members is depicted in Fig. 7. The system is initially at rest and is put into motion by a concentrated moment at its right support. The value of the moment varies linearly with time, starting from 0, peaking 5 Nm at time 0.125 s, and vanishing at time 0.25 s. The dynamic response within the first second of motion is observed. The system is modelled by four finite elements (Fig. 7) with the fourth-order interpolation of strain. The system consists of two rotational joints and one translational joint. The time step is $\Delta t = 0.001\,\text{s}$.

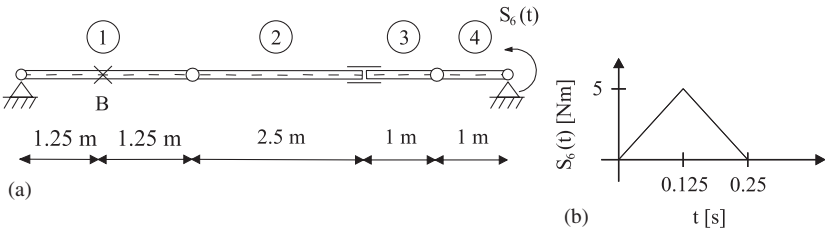

Fig. 7. Four-body system: (a) geometry, (b) time variation of torque S_6. Material and cross-sectional data: $EA = 5.65 \times 10^5\,\text{N}$, $GA_s = 1.4038 \times 10^5\,\text{N}$, $EI_y = 3.040\,\text{Nm}^2$, $\rho A = 0.0135\,\text{kg/m}$, $\rho I_y = 1.125 \times 10^{-6}\,\text{kg m}$.

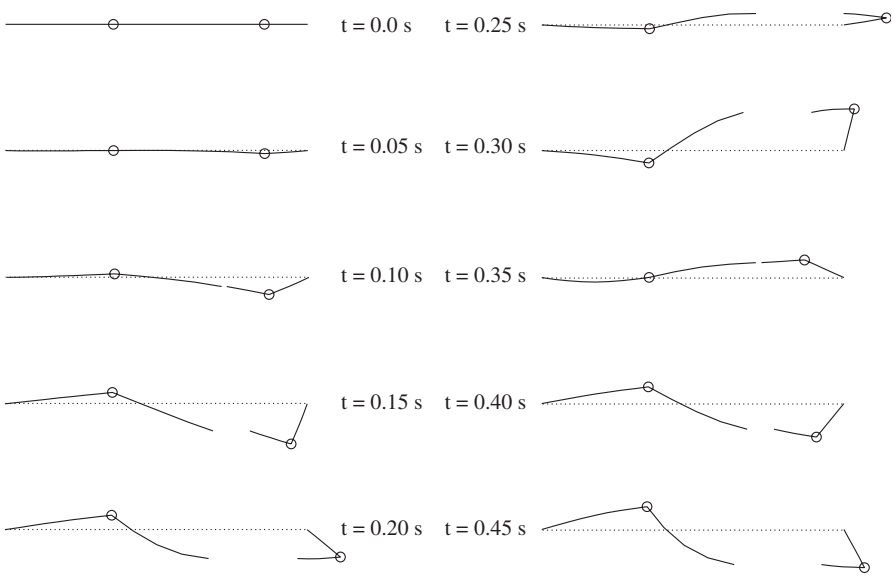

Fig. 8. Four-body system. The sequence of deformed shapes in time interval $[0, 0.45]\,\text{s}$. The sequence is depicted in 0.05 s intervals.

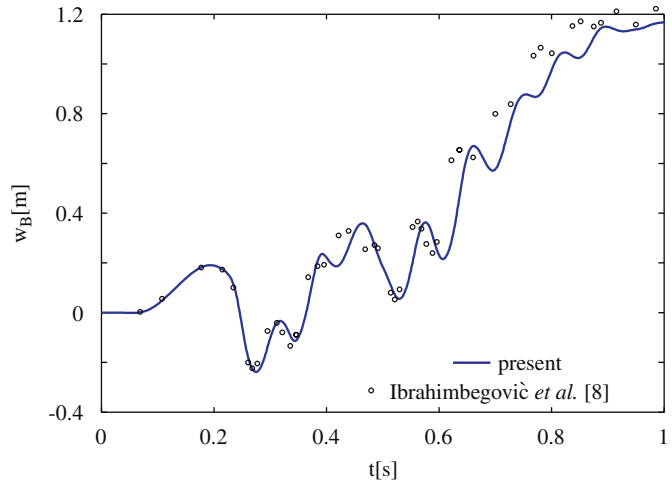

Fig. 9. The time variation of vertical displacement w_B. Solid line: present formulation, circles: Ref. [8].

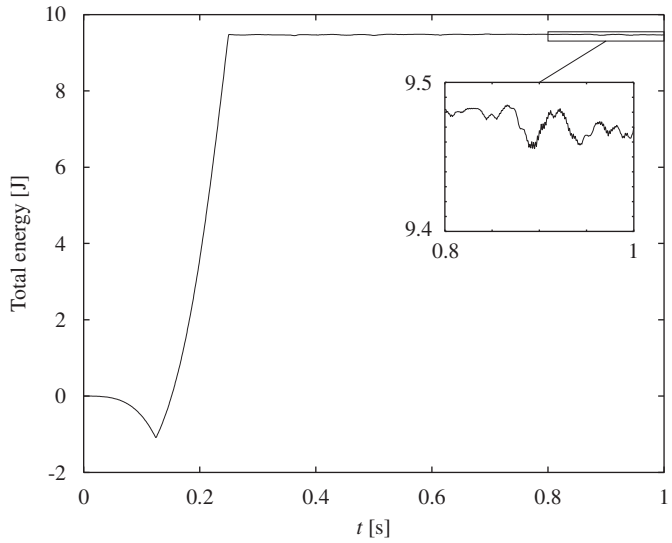

Fig. 10. Time variation of total energy of the system. In the inserted detail, a closer view of the energy variation with time is shown for $t \in [0.8, 1]$ s. Oscillations are clearly visible.

Ibrahimbegović and Mamouri used 20 two-node (linear) displacement-based elements with selectively reduced integration to model the system [8] and their energy conserving time integration scheme.

Two quantities are being observed in this example: the vertical displacement at point B and the mechanical energy of the system. The mechanical energy of the system is calculated as a sum of kinetic and potential energies, i.e. using Eqs. (5)–(6). The system undergoes interesting deformed configurations; some of them are depicted in Fig. 8. The time variation of the vertical displacement at point B is compared with Ref. [8] in Fig. 9. The time variation of the mechanical energy is shown in Fig. 10. Some disagreement in the vertical displacement at point B is observed between the two formulations. They are due to the coarse finite-element mesh and/or low interpolation degree employed in Ref. [8].

The system represents a stiff problem, because it involves very different frequencies, related to bending and axial vibrations. The time integration scheme proposed in Ref. [8] appears to be ideally suited for such problems as it enforces the energy conservation, and consequently, assures the unconditional stability of the

time-integration schemes. By contrast, the midpoint time integration scheme used in our formulation does not automatically preserve the mechanical energy (Fig. 10) and is, consequently, a conditionally stable integration scheme. Therefore, it is not well suited for stiff systems. This is demonstrated in a sudden onset of violent oscillations, blow up of the mechanical energy and loss of convergence of the Newton procedure shortly after. As clearly seen in Fig. 10, the oscillations of the total energy are not significant until 1 s. At about 1.8 s the mechanical energy blows up and Newton's iteration breaks down.

7. Conclusions

The present paper proposes a new finite-element formulation for the large deformation, dynamic analysis of highly flexible elastic planar beam-like multibody systems. This formulation, which allows a point-wise imposition of cross-sectional equilibrium equations and an arbitrary order of interpolation polynomials, is strain based. The main contribution is the introduction of a special algorithm for the numerical integration, which helps to avoid nested integrations and saves computing time.

The numerical examples show that: (i) the accuracy of the proposed finite elements is comparable with the accuracy of the displacement-based elements; (ii) the formulation is computationally much more efficient than the one given in Ref. [22]; for the numerical examples presented in the paper, the computational times appeared to be roughly 10-times smaller than those of the formulation by Gams et al. [22]; and (iii) the midpoint time integration scheme in conjunction with the present strain-based finite elements is conditionally stable.

Acknowledgement

The work of M. Gams was financially supported by the Agency of research of the Republic of Slovenia under contract 8311-03-831622. The support is gratefully acknowledged.

References

[1] O.A. Bauchau, N.J. Theron, Energy decaying scheme for nonlinear beam model, *Computer Methods in Applied Mechanics and Engineering* 134 (1996) 37–56.
[2] P. Betsch, P. Steinmann, Constrained dynamics of geometrically exact beams, *Computational Mechanics* 31 (2003) 49–59.
[3] M.A. Crisfield, J. Shi, A co-rotational element/time-integration strategy for non-linear dynamics, *International Journal for Numerical Methods in Engineering* 37 (1994) 1897–1931.
[4] M.A. Crisfield, U. Galvanetto, G. Jelenić, Dynamics of 3-D co-rotational beams, *Computational Mechanics* 20 (1997) 507–519.
[5] S. von Dombrowski, Analysis of large flexible body deformation in multibody systems using absolute coordinates, *Multibody System Dynamics* 8 (2003) 409–432.
[6] K.E. Dufva, J.T. Sopanen, A.M. Mikkola, A two-dimensional shear deformable beam element based on the absolute nodal coordinate formulation, *Journal of Sound and Vibration* 280 (2005) 719–738.
[7] K.M. Hsiao, J.Y. Jang, Dynamic analysis of planar flexible mechanisms by co-rotational formulation, *Computer Methods in Applied Mechanics and Engineering* 87 (1991) 1–14.
[8] A. Ibrahimbegović, A.S. Mamouri, Nonlinear dynamics of flexible beams in planar motion: Formulation and time stepping scheme for stiff problems, *Computers and Structures* 70 (1999) 1–22.
[9] M. Iura, S.N. Atluri, Dynamic analysis of planar flexible beams with finite rotations by using inertial and rotating frames, *Computers and Structures* 55 (1995) 453–462.
[10] M.A. Omar, A.A. Shabana, A two-dimensional shear deformable beam for large rotation and deformation problems, *Journal of Sound and Vibrations* 243 (3) (2001) 565–576.
[11] C. Sansour, J. Sansour, P. Wriggers, A finite element approach to the chaotic motion of geometrically exact rods undergoing in-plane deformations, *Nonlinear Dynamics* 11 (1996) 189–212.
[12] A.A. Shabana, *Dynamics of Multibody Systems*, second ed., Cambridge University Press, Cambridge, 1998.
[13] A.A. Shabana, Definition of the slopes and the finite element absolute nodal coordinate formulation, *Multibody System Dynamics* 1 (3) (1997) 339–348.
[14] J.C. Simo, L. Vu-Quoc, On the dynamics of flexible beams under large overall motions—the plane case: part I and Part II, *ASME Journal of Applied Mechanics* 53 (1986) 849–863.
[15] J.C. Simo, N. Tarnow, M. Doblare, Non-linear dynamics of three-dimensional rods: exact energy and momentum conserving algorithms, *International Journal for Numerical Methods in Engineering* 38 (1995) 1431–1473.

[16] N. Stander, E. Stein, An energy-conserving planar finite beam element for dynamics of flexible mechanisms, *Engineering Computations* 13 (6) (1996) 60–85.
[17] S. Bratina, M. Saje, I. Planinc, On materially and geometrically non-linear analysis of reinforced concrete planar beams, *International Journal of Solids and Structures* 41 (2004) 7181–7207.
[18] S. Bratina, B. Čas, M. Saje, I. Planinc, Numerical modelling of behaviour of reinforced concrete columns in fire and comparison with Eurocode 2, *International Journal of Solids and Structures* 42 (21–22) (2005) 5715–5733.
[19] D. Zupan, M. Saje, Finite-element formulation of geometrically exact three-dimensional beam theories based on interpolation of strain measures, *Computer Methods in Applied Mechanics and Engineering* 192 (2003) 5209–5248.
[20] B. Čas, M. Saje, I. Planinc, Non-linear finite element analysis of composite planar frames with an interlayer slip, *Computers and Structures* 82 (2004) 1901–1912.
[21] B. Čas, S. Bratina, M. Saje, I. Planinc, Non-linear analysis of composite steel-concrete beams with incomplete interaction, *Steel and Composite Structures* 4 (2004) 489–507.
[22] M. Gams, M. Saje, S. Srpčič, I. Planinc, Finite element dynamic analysis of geometrically exact beams, Computers and Structures (2006) doi:10.1016/j.compstruc.2006.08.081.
[23] E. Reissner, On one-dimensional finite-strain beam theory: the plane problem, *Journal of Applied Mathematics and Physics (ZAMP)* 23 (1972) 795–804.
[24] I. Planinc, M. Saje, B. Čas, On local stability condition in planar beam finite element, *Structural Engineering and Mechanics* 12 (2001) 507–526.
[25] M. Géradin, A. Cardona, *Flexible Multibody Dynamics. A Finite Element Approach*, Wiley, New York, 2001.
[26] B. Vratanar, M. Saje, A consistent equilibrium in a cross-section of an elastic-plastic beam, *International Journal of Solids and Structures* 36 (1999) 311–337.
[27] G. Jelenić, Dynamics of Plane Hyperelastic Beams with Finite Strains, MS Thesis, Faculty of Civil and Geodetic Engineering, University of Ljubljana, 1990 (in Slovenian).
[28] M. Saje, I. Planinc, G. Turk, B. Vratanar, A kinematically exact finite element formulation of planar elastic-plastic beam, *Computer Methods in Applied Mechanics and Engineering* 144 (1997) 125–151.
[29] B. Vratanar, The Geometrically Exact Dynamics of Planar Beams, PhD Thesis, Faculty of Civil and Geodetic Engineering, University of Ljubljana, 1998 (in Slovenian).
[30] T.-Y. Rong, A.-Q. Lu, Generalized mixed variational principles and solutions of ill-conditioned problems in computational mechanics. Part II: shear locking, *Computer Methods in Applied Mechanics and Engineering* 192 (2003) 4981–5000.